Inorganic Chemistry
Article

Inorg. Chem. **2010**, *49*, 1325–1336 **1325**
DOI: 10.1021/ic901480y

Binding of Higher Alcohols onto Mn_{12} Single-Molecule Magnets (SMMs): Access to the Highest Barrier Mn_{12} SMM

Christos Lampropoulos,[†] Gage Redler,[‡] Saiti Data,[‡] Khalil A. Abboud,[†] Stephen Hill,*[,‡,§] and George Christou*[,†]

[†]*Department of Chemistry, and* [‡]*Department of Physics, University of Florida, Gainesville, Florida 32611, and* [§]*Department of Physics and National High Magnetic Field Laboratory, Florida State University, Tallahassee, Florida 32310*

Received July 25, 2009

Two new members of the Mn_{12} family of single-molecule magnets (SMMs), $[Mn_{12}O_{12}(O_2CCH_2Bu^t)_{16}(Bu^tOH)(H_2O)_3]\cdot 2Bu^tOH$ (**3**·2Bu^{t}OH) and $[Mn_{12}O_{12}(O_2CCH_2Bu^t)_{16}(C_5H_{11}OH)_4]$ (**4**) ($C_5H_{11}OH$ is 1-pentanol), are reported. They were synthesized from $[Mn_{12}O_{12}(O_2CMe)_{16}(H_2O)_4]\cdot 2MeCO_2H\cdot 4H_2O$ (**1**) by carboxylate substitution and crystallization from the appropriate alcohol-containing solvent. Complexes **3** and **4** are new members of the recently established $[Mn_{12}O_{12}(O_2CCH_2Bu^t)_{16}(solv)_4]$ (solv = H_2O, alcohols) family of SMMs. Only one bulky Bu^{t}OH can be accommodated into **3**, and even this causes significant distortion of the $[Mn_{12}O_{12}]$ core. Variable-temperature, solid-state alternating current (AC) magnetization studies were carried out on complexes **3** and **4**, and they established that both possess an $S = 10$ ground state spin and are SMMs. However, the magnetic behavior of the two compounds was found to be significantly different, with **4** showing out-of-phase AC peaks at higher temperatures than **3**. High-frequency electron paramagnetic resonance (HFEPR) studies were carried out on single crystals of **3**·2Bu^{t}OH and **4**, and these revealed that the axial zero-field splitting constant, D, is very different for the two compounds. Furthermore, it was established that **4** is the Mn_{12} SMM with the highest kinetic barrier (U_{eff}) to date. The results reveal alcohol substitution as an additional and convenient means to affect the magnetization relaxation barrier of the Mn_{12} SMMs without major change to the ligation or oxidation state.

Introduction

Single-molecule magnets (SMMs) are individual molecules that function as nanoscale magnetic particles.[1−3] They are typically polynuclear assemblies of magnetically coupled, paramagnetic metal ions, usually bridged by oxides and surrounded by a shell of organic ligands that serves to isolate the magnetic core from neighboring ones and also stabilize them from polymerization to larger particles or three-dimensional (3-D) metal oxides. Their molecular nature brings valuable advantages to nanomagnetism, since molecular crystals provide 3-D organizations of monodisperse particles of a well-defined size and often of a single, uniform orientation.[1] Their behavior as nanomagnets arises from their intrinsic, intramolecular properties of a large ground state spin (S) and an anisotropy resulting from the precise details of their constituent structure. The anisotropy is of the Ising (easy-axis) type, and is reflected in a negative D value, where D is the second order axial zero-field splitting (ZFS) parameter. Potential applications of SMMs range from ultrahigh-density memory storage devices, through spintronics, to quantum computation owing to their combination of classical and quantum properties.[4] Furthermore, SMMs have been exceptionally useful as models for studying complex quantum phenomena, such as quantum tunneling of the magnetization,[5] spin parity, quantum

*To whom correspondence should be addressed. E-mail: christou@chem.ufl.edu (G.C.), shill@magnet.fsu.edu (S.H.). Phone: (+1) 352-392-8314 (G.C.), (+1) 850-644-1647 (S.H.).

(1) (a) Christou, G.; Gatteschi, D.; Hendrickson, D. N.; Sessoli, R. *MRS Bull.* **2000**, *25*, 66. (b) Aromi, G.; Brechin, E. K. *Struct. Bonding* (*Berlin*) **2006**, *122*, 1. (c) Christou, G. *Polyhedron* **2005**, *24*, 2065.

(2) (a) Sessoli, R.; Tsai, H. L.; Schake, A. R.; Wang, S.; Vincent, J. B.; Folting, K.; Gatteschi, D.; Christou, G.; Hendrickson, D. N. *J. Am. Chem. Soc.* **1993**, *115*, 1804. (b) Sessoli, R.; Gatteschi, D.; Caneschi, A.; Novak, M. A. *Nature* **1993**, *365*, 141.

(3) Christou, G. *Polyhedron* **2005**, *24*, 2065.

(4) (a) Bogani, L.; Wernsdorfer, W. *Nat. Mater.* **2008**, *7*, 179. (b) Leuenberger, M. N.; Loss *Nature* **2001**, *410*, 789. (c) Tejada, J.; Chudnovsky, E. M.; del Barco, E.; Hernandez, J. M.; Spiller, T. P. *Nanotechnology* **2001**, *12*, 181.

(5) (a) Friedman, J. R.; Sarachik, M. P.; Tejada, J.; Ziolo, R. *Phys. Rev. Lett.* **1996**, *76*, 3830. (b) Morello, A.; Bakharev, O. N.; Brom, H. B.; de Jongh, L. J. *Polyhedron* **2003**, *22*, 1745. (c) Brechin, E. K.; Boskovic, C.; Wernsdorfer, W.; Yoo, J.; Yamaguchi, A.; Sanudo, E. C.; Concolino, T. R.; Rheingold, A. L.; Ishimoto, H.; Hendrickson, D. N.; Christou, G. *J. Am. Chem. Soc.* **2002**, *124*, 9710. (d) Gatteschi, D.; Sessoli, R. *Angew. Chem., Int. Ed.* **2003**, *42*, 268. (e) Caneschi, A.; Ohm, T.; Paulsen, C.; Rovai, D.; Sangregorio, C.; Sessoli, R. *J. Magn. Magn. Mater.* **1998**, *177−181*, 1330. (f) del Barco, E.; Kent, A. D.; Hill, S.; North, J. M.; Dalal, N. S.; Rumberger, E. M.; Hendrickson, D. N.; Chakov, N.; Christou, G. *J. Low Temp. Phys.* **2005**, *140*, 119. (g) Friedman, J. R.; Sarachik, M. P.; Tejada, J.; Ziolo, R. *Phys. Rev. Lett.* **1996**, *76*, 3830.

Published on Web 01/21/2010

phase interference,[6] and quantum superpositions,[7a] as well as electron paramagnetic resonance (EPR) and ^{55}Mn NMR spectra,[7b−g] and exotic physical properties such as magnetic deflagration.[8] For such reasons, they have been under study by a wide range of scientists spanning many disciplines.

The first SMM was $[Mn_{12}O_{12}(O_2CMe)_{16}(H_2O)_4]\cdot 2MeCO_2H\cdot 4H_2O$ (**1**), which has since been expanded to a large family of related Mn_{12} complexes.[2,9] In addition, a large number of other structural types of SMMs have since been discovered, most of which are based on manganese:[10] these include several heterometallic 3d/4f clusters,[11] homometallic first-row 3d metal clusters,[12] and homometallic 4f clusters.[13]

The $[Mn_{12}O_{12}(O_2CMe)_{16}(H_2O)_4]$ family remains the most studied and best understood, having been the focus of many physical and spectroscopic studies for reasons that include the high symmetry of their Mn_{12} core, their usually well-isolated spin ground state, their ease of preparation from cheap materials, and their stability in the solid state and in solution, which has allowed their ready modification in a variety of ways.[14] In fact, a number of modifications to the Mn_{12} structure have been achieved over the years, including carboxylate substitution,[15,16] replacement of carboxylate with anions of other organic and inorganic acids, and the

(6) (a) Wernsdorfer, W.; Chakov, N. E.; Christou, G. *Phys. Rev. Lett.* **2005**, *95*, 037203/1. (b) Wernsdorfer, W.; Sessoli, R. *Science* **1999**, *284*, 133. (c) Wernsdorfer, W.; Soler, M.; Christou, G.; Hendrickson, D. N. *J. Appl. Phys.* **2002**, *91*, 7164.

(7) (a) Hill, S.; Edwards, R. S.; Aliaga-Alcalde, N.; Christou, G. *Science* **2003**, *302*, 1015. (b) Macia, F.; Lawrence, J.; Hill, S.; Hernandez, J. M.; Tejada, J.; Santos, P. V.; Lampropoulos, C.; Christou, G. *Phys. Rev. B* **2008**, *77*, 020403. (c) Harter, A. G.; Chakov, N. E.; Achey, R.; Reyes, A.; Kuhns, P.; Christou, G.; Dalal, N. S. *Polyhedron* **2005**, *24*, 2346. (d) Harter, A. G.; Lampropoulos, C.; Murugesu, M.; Kuhns, P.; Reyes, A.; Christou, G.; Dalal, N. S. *Polyhedron* **2007**, 2320. (e) Petukhov, K.; Hill, S.; Chakov, N. E.; Abboud, K. A.; Christou, G. *Phys. Rev. B* **2004**, *70*, 054426. (f) Perenboom, J.; Brooks, J. S.; Hill, S.; Hathaway, T.; Dalal, N. S. *Phys. Rev. B* **1998**, *58*, 330. (g) Park, K.; Novotny, M. A.; Dalal, N. S.; Hill, S.; Rikvold, P. A. *Phys. Rev. B* **2002**, *66*, 020403.

(8) (a) Jaafar, R.; McHugh, S.; Suzuki, Y.; Sarachik, M. P.; Myasoedov, Y.; Zeldov, E.; Shtrikman, H.; Bagai, R.; Christou, G. *J. Magn. Magn. Mater.* **2008**, *320*, 695–698. (b) McHugh, S.; Jaafar, R.; Sarachik, M. P.; Myasoedov, Y.; Finkler, A.; Shtrikman, H.; Zeldov, E.; Bagai, R.; Christou, G. *Phys. Rev. B* **2007**, *76*, 172410. (c) Suzuki, Y.; Sarachik, M. P.; Chudnovsky, E. M.; McHugh, S.; Gonzalez-Rubio, R.; Avraham, N.; Myasoedov, Y.; Zeldov, E.; Shtrikman, H.; Chakov, N. E.; Christou, G. *Phys. Rev. Lett.* **2005**, *95*, 147201. (d) Macià, F.; Hernandez, J. M.; Tejada, J.; Datta, S.; Hill, S.; Lampropoulos, C.; Christou, G. *Phys. Rev. B* **2009**, *79*, 092403.

(9) Lis, T. *Acta Crystallogr., Sect. B: Struct. Sci.* **1980**, *36*, 2042.

(10) (a) Aliaga-Alcalde, N.; Edwards, R. S.; Hill, S. O.; Wernsdorfer, W.; Folting, K.; Christou, G. *J. Am. Chem. Soc.* **2004**, *126*, 12503. (b) Foguet-Albiol, D.; O'Brien, T. A.; Wernsdorfer, W.; Moulton, B.; Zaworotko, M. J.; Abboud, K. A.; Christou, G. *Angew. Chem., Int. Ed.* **2005**, *44*, 897. (c) King, P.; Wernsdorfer, W.; Abboud, K. A.; Christou, G. *Inorg. Chem.* **2005**, *44*, 8659. (d) Murugesu, M.; Habrych, M.; Wernsdorfer, W.; Abboud, K. A.; Christou, G. *J. Am. Chem. Soc.* **2004**, *126*, 4766. (e) Soler, M.; Wernsdorfer, W.; Folting, K.; Pink, M.; Christou, G. *J. Am. Chem. Soc.* **2004**, *126*, 2156. (f) Stamatatos, T. C.; Foguet-Albiol, D.; Stoumpos, C. C.; Raptopoulou, C. P.; Terzis, A.; Wernsdorfer, W.; Perlepes, S. P.; Christou, G. *J. Am. Chem. Soc.* **2005**, *127*, 15380. (g) Tasiopoulos, A. J.; Wernsdorfer, W.; Abboud, K. A.; Christou, G. *Angew. Chem., Int. Ed.* **2004**, *43*, 6338. (h) Tasiopoulos, A. J.; Vinslava, A.; Wernsdorfer, W.; Abboud, K. A.; Christou, G. *Angew. Chem., Int. Ed.* **2004**, *43*, 2117. (i) Stamatatos, T. C.; Abboud, K. A.; Wernsdorfer, W.; Christou, G. *Angew. Chem., Int. Ed.* **2008**, *47*, 6694. (j) Murugesu, M.; Takahashi, S.; Wilson, A.; Abboud, K. A.; Wernsdorfer, W.; Hill, S.; Christou, G. *Inorg. Chem.* **2008**, *47*, 4095. (k) Brockman, J. T.; Stamatatos, T. C.; Wernsdorfer, W.; Abboud, K. A.; Christou, G. *Inorg. Chem.* **2007**, *46*, 9160. (l) Milios, C. J.; Inglis, R.; Vinslava, A.; Bagai, R.; Wernsdorfer, W.; Parsons, S.; Perlepes, S. P.; Christou, G.; Brechin, E. K. *J. Am. Chem. Soc.* **2007**, *129*, 12505. (m) Milios, C. J.; Inglis, R.; Bagai, R.; Wernsdorfer, W.; Collins, A.; Moggach, S.; Parsons, S.; Perlepes, S. P.; Christou, G.; Brechin, E. K. *Chem. Commun.* **2007**, 3476. (n) Stamatatos, T. C.; Foguet-Albiol, D.; Lee, S.-C.; Stoumpos, C. C.; Raptopoulou, C. P.; Terzis, A.; Wernsdorfer, W.; Hill, S. O.; Perlepes, S. P.; Christou, G. *J. Am. Chem. Soc.* **2007**, *129*, 9484. (o) Milios, C. J.; Vinslava, A.; Wernsdorfer, W.; Moggach, W.; Parsons, S.; Perlepes, S. P.; Christou, G.; Brechin, E. K. *J. Am. Chem. Soc.* **2007**, *129*, 2754. (p) Milios, C. J.; Vinslava, A.; Wood, P. A.; Parsons, S.; Wernsdorfer, W.; Christou, G.; Perlepes, S. P.; Brechin, E. K. *J. Am. Chem. Soc.* **2007**, *129*, 8. (q) Ritchie, C.; Ferguson, A.; Nojiri, H.; Miras, H. N.; Song, Y.-F.; Long, D.-L.; Burkholder, E.; Murrie, M.; Kögerler, P.; Brechin, E. K.; Cronin, L. *Angew. Chem., Int. Ed.* **2008**, *47*, 5609. (r) Miyasaka, H.; Clérac, R.; Wernsdorfer, W.; Lecren, L.; Bonhomme, C.; Sugiura, K.-i.; Yamashita, M. *Angew. Chem., Int. Ed.* **2004**, *43*, 2801. (s) Milios, C. J.; Raptopoulou, C. P.; Terzis, A.; Lloret, F.; Vicente, R.; Perlepes, S. P.; Escuer, A. *Angew. Chem., Int. Ed.* **2004**, *43*, 210. (t) Berlinguette, C. P.; Vaughn, D.; Cañada-Vilalta, C.; Galán-Mascarós, J. R.; Dunbar, K. R. *Angew. Chem., Int. Ed.* **2003**, *42*, 1523. (u) Yang, C.-I.; Wernsdorfer, W.; Lee, G.-H.; Tsai, H.-L. *J. Am. Chem. Soc.* **2007**, *129*, 456.

(11) (a) Mishra, A.; Wernsdorfer, W.; Abboud, K. A.; Christou, G. *J. Am. Chem. Soc.* **2004**, *126*, 15648. (b) Mishra, A.; Wernsdorfer, W.; Parsons, S.; Christou, G.; Brechin, E. K. *Chem. Commun.* **2005**, 2086. (c) Tasiopoulos, A. J.; Wernsdorfer, W.; Moulton, B.; Zaworotko, M. J.; Christou, G. *J. Am. Chem. Soc.* **2003**, *125*, 15274. (d) Stamatatos, T. C.; Teat, S. J.; Wernsdorfer, W.; Christou, G. *Angew. Chem., Int. Ed.* **2009**, *48*, 521. (e) Zaleski, C. M.; Depperman, E. C.; Kampf, J. W.; Kirk, M. L.; Pecoraro, V. L. *Angew. Chem., Int. Ed.* **2004**, *43*, 3912. (f) Mori, F.; Nyui, T.; Ishida, T.; Nogami, T.; Choi, K.-Y.; Nojiri, H. *J. Am. Chem. Soc.* **2006**, *128*, 1440. (g) Mereacre, V. M.; Ako, A. M.; Clerac, R.; Wernsdorfer, W.; Filoti, G.; Bartolome, J.; Anson, C. E.; Powell, A. K. *J. Am. Chem. Soc.* **2007**, *129*, 9248. (h) Ferbinteanu, M.; Kajiwara, T.; Choi, K.-Y.; Nojiri, H.; Nakamoto, A.; Kojima, N.; Cimpoesu, F.; Fujimura, Y.; Takaishi, S.; Yamashita, M. *J. Am. Chem. Soc.* **2006**, *128*, 9008. (i) Osa, S.; Kido, T.; Matsumoto, N.; Re, N.; Pochaba, A.; Mrozinski, J. *J. Am. Chem. Soc.* **2004**, *126*, 420. (j) Mukherjee, S.; Daniels, M. R.; Bagai, R.; Abboud, K. A.; Christou, G.; Lampropoulos, C. *Polyhedron* **2010**, *29*, 54.

(12) (a) Oshio, H.; Hoshino, N.; Ito, T. *J. Am. Chem. Soc.* **2000**, *122*, 12602. (b) Castro, S. L.; Sun, Z.; Grant, C. M.; Bollinger, J. C.; Hendrickson, D. N.; Christou, G. *J. Am. Chem. Soc.* **1998**, *120*, 2365. (c) Bagai, R.; Wernsdorfer, W.; Abboud, K. A.; Christou, G. *J. Am. Chem. Soc.* **2007**, *129*, 12918. (d) Barra, A. L.; Caneschi, A.; Cornia, A.; Fabrizi de Biani, F.; Gatteschi, D.; Sangregorio, C.; Sessoli, R.; Sorace, L. *J. Am. Chem. Soc.* **1999**, *121*, 5302. (e) Accorsi, S.; Barra, A.-L.; Caneschi, A.; Chastanet, G.; Cornia, A.; Fabretti, A. C.; Gatteschi, D.; Mortalo, C.; Olivieri, E.; Parenti, F.; Rosa, P.; Sessoli, R.; Sorace, L.; Wernsdorfer, W.; Zobbi, L. *J. Am. Chem. Soc.* **2006**, *128*, 4742. (f) Murrie, M.; Teat, S. J.; Stoeligckli-Evans, H.; Güdel, H. U. *Angew. Chem., Int. Ed.* **2003**, *42*, 4653. (g) Cornia, A.; Fabretti, A. C.; Garrisi, P.; Mortalò, C.; Bonacchi, D.; Gatteschi, D.; Sessoli, R.; Sorace, L.; Wernsdorfer, W.; Barra, A.-L. *Angew. Chem., Int. Ed.* **2004**, *43*, 1136. (h) Cornia, A.; Fabretti, A. C.; Garrisi, P.; Mortalò, C.; Bonacchi, D.; Gatteschi, D.; Sessoli, R.; Sorace, L.; Wernsdorfer, W.; Barra, A.-L. *Angew. Chem., Int. Ed.* **2004**, *43*, 1136. (i) Bertaina, S.; Gambarelli, S.; Mitra, T.; Tsukerblat, B.; Muller, A.; Barbara, B. *Nature* **2008**, *453*, 203. (j) Powell, G. W.; Lancashire, H. N.; Brechin, E. K.; Collison, D.; Heath, S. L.; Mallah, T.; Wernsdorfer, W. *Angew. Chem., Int. Ed.* **2004**, *43*, 6581.

(13) (a) Lin, P.-H.; Burchell, T. J.; Clérac, R.; Murugesu, M. *Angew. Chem., Int. Ed.* **2008**, *47*, 8848. (b) Hussain, B.; Savard, D.; Burchell, T. J.; Wernsdorfer, W.; Murugesu, M. *Chem. Commun.* **2009**, 1100. (c) AlDamen, M. A.; Clemente-Juan, J. M.; Coronado, E.; Marti -Gastaldo, C.; Gaita-Arinfo, A. *J. Am. Chem. Soc.* **2008**, *130*, 8874. (d) Ishikawa, N.; Sugita, M.; Wernsdorfer, W. *J. Am. Chem. Soc.* **2005**, *127*, 3650.

(14) Bagai, R.; Christou, G. *Chem. Soc. Rev.* **2009**, *38*, 1011 and references therein.

(15) (a) Boyd, P. D. W.; Li, Q.; Vincent, J. B.; Folting, K.; Chang, H. R.; Streib, W. E.; Huffman, J. C.; Christou, G.; Hendrickson, D. N. *J. Am. Chem. Soc.* **1988**, *110*, 8537. (b) Eppley, H. J.; Tsai, H.-L.; de Vries, N.; Folting, K.; Christou, G.; Hendrickson, D. N. *J. Am. Chem. Soc.* **1995**, *117*, 301. (c) Aubin, S. M. J.; Sun, Z.; Hendrickson, D. N.; Aubin, S. M. J.; Guzei, I. A.; Rheingold, A. L.; Christou, G. *Chem. Commun.* **1997**, 2239. (d) Sun, Z.; Ruiz, D.; Dilley, N. R.; Soler, M.; Ribas, J.; Folting, K.; Maple, M. B.; Christou, G.; Hendrickson, D. N. *Chem. Commun.* **1999**, 1973. (e) Aubin, S. M. J.; Eppley, H. J.; Guzei, I. A.; Folting, K.; Gantzel, P. K.; Rheingold, A. L.; Christou, G.; Hendrickson, D. N. *Inorg. Chem.* **2001**, *40*, 2127. (f) Kuroda-Sowa, T.; Nakano, M.; Christou, G.; Hendrickson, D. N. *Polyhedron* **2001**, *20*, 1529. (g) Soler, M.; Artus, P.; Folting, K.; Huffman, J. C.; Hendrickson, D. N.; Christou, G. *Inorg. Chem.* **2001**, *40*, 4902. (h) Boskovic, C.; Pink, M.; Huffman, J. C.; Hendrickson, D. N.; Christou, G. *J. Am. Chem. Soc.* **2001**, *123*, 9914. (i) Eppley, H. J.; Christou, G. *Inorg. Synth.* **2002**, *33*, 61. (j) Chakov, N. E.; Wernsdorfer, W.; Abboud, K. A.; Hendrickson, D. N.; Christou, G. *Dalton Trans.* **2003**, 2243. (k) Brockman, J. T.; Abboud, K. A.; Hendrickson, D. N.; Christou, G. *Polyhedron* **2003**, *22*, 1759.

(16) Chakov, N. E.; Lawrence, J.; Harter, A. G.; Hill, S. O.; Dalal, N. S.; Wernsdorfer, W.; Abboud, K. A.; Christou, G. *J. Am. Chem. Soc.* **2006**, *128*, 6975.

preparation of 1-,[17] 2-[18] and 3-electron reduced species,[19] among others.[20] As such, it has been the main source of information to date on the SMM phenomenon.

Recently, bulky carboxylates have been introduced into $[Mn_{12}O_{12}(O_2CR)_{16}(H_2O)_4]$ complexes, which among other things have increased the intermolecular separations and minimized intermolecular communication.[20] One of these has been *tert*-butylacetate ($Bu^tCH_2CO_2^-$), giving $[Mn_{12}O_{12}(O_2CCH_2Bu^t)_{16}(H_2O)_4]$,[20a] and subsequently $[Mn_{12}O_{12}(O_2CCH_2Bu^t)_{16}(MeOH)_4]\cdot MeOH$ (**2**·MeOH) on crystallization from a MeOH-containing medium.[21] Complex **2** crystallizes, like **1**, in a high symmetry tetragonal space group with the complex having imposed S_4 (axial) symmetry, and thus proved very attractive for studies by a variety of techniques. We have recently extended this work to higher alcohols to assess what influence their different bulk and/or basicity might have on the magnetic properties of the Mn_{12} SMM. We herein report the syntheses, crystal structures, magnetic properties, and high-frequency EPR (HFEPR) spectral data for two new Mn_{12} derivatives, $[Mn_{12}O_{12}(O_2CCH_2Bu^t)_{16}(Bu^tOH)(H_2O)_3]\cdot 2Bu^tOH$ (**3**) and $[Mn_{12}O_{12}(O_2CCH_2Bu^t)_{16}(C_5H_{11}OH)_4]$ (**4**).

Experimental Section

Synthesis. All manipulations were performed under aerobic conditions using materials as received, except where otherwise noted. $[Mn_{12}O_{12}(O_2CMe)_{16}(H_2O)_4]\cdot 2MeCO_2H\cdot 4H_2O$ (**1**) was prepared as described elsewhere.[2a,22]

$[Mn_{12}O_{12}(O_2CCH_2Bu^t)_{16}(Bu^tOH)(H_2O)_3]$ (3). Freshly prepared crystals of complex **1** (0.50 g, 0.24 mmol) were dissolved in Bu^tOH (40 mL), and $Bu^tCH_2CO_2H$ (5 mL) was added under continuous magnetic stirring. The reaction mixture was heated at ~40 °C for 30 min, and then allowed to cool to room temperature. The solution was filtered, and the filtrate was allowed to stand undisturbed for 4 days at ambient temperature, during which time large black needles of **3**·2Bu^tOH formed in 60% yield. Samples for X-ray crystallography and alternating current (AC) magnetometry were kept wet with mother liquor until needed, otherwise they were filtered, washed with a little Bu^tOH and Et_2O, and dried in vacuo; vacuum-dried solid analyzed as solvent-free. Anal. Calcd (found) for **3**: C, 42.56 (42.31); H, 6.86 (6.92); N, 0.00 (0.02) %. Selected IR data (KBr, cm^{-1}): 3598 (m), 3387 (m), 1559 (s), 1508 (s), 1449 (s), 1388 (s), 1333 (s), 1256 (w), 1029 (w), 958 (w), 714 (m), 674 (s), 640 (s), 610 (s), 563 (m), 518 (m), 409 (w).

$[Mn_{12}O_{12}(O_2CCH_2Bu^t)_{16}(C_5H_{11}OH)_4]$ (4). Freshly prepared crystals of complex **1** (0.50 g, 0.24 mmol) were dissolved in 1-pentanol (40 mL), and $Bu^tCH_2CO_2H$ (5 mL) was added under continuous magnetic stirring. The reaction mixture was heated at ~40 °C for 30 min, and then allowed to cool to room temperature. The solution was filtered, and the filtrate was allowed to stand undisturbed for 10 days, during which time large black needles of **4** slowly grew in 80% yield. Samples for X-ray crystallography and AC magnetometry were kept wet with mother liquor until needed, otherwise they were filtered, washed with a little *n*-pentanol and Et_2O, and dried in vacuo. Anal. Calcd (found) for **4**: C, 45.10 (44.92); H, 7.31 (6.95); N, 0.00 (0.01) %. Selected IR data (KBr, cm^{-1}): 3420 (w), 2954 (s), 2867 (m), 1587 (s), 1518 (s), 1413 (s), 1366 (s), 1306 (w), 1275 (w), 1234 (m), 1199 (w), 1140 (w), 1050 (w), 977 (w), 906 (w), 705 (m), 637 (s), 601 (m), 560 (m), 465 (w).

X-ray Crystallography. Data were collected at 173 K on a Siemens SMART PLATFORM equipped with a CCD area detector and a graphite monochromator utilizing Mo Kα radiation (λ = 0.71073 Å). Suitable crystals of **3**·2Bu^tOH and **4** were attached to a glass fiber using silicone grease and transferred to the goniostat where they were cooled to −100 °C for characterization and data collection. The structures were solved by Direct Methods in SHELXTL6, and refined on F^2 using full-matrix least-squares. The non-H atoms were treated anisotropically, whereas the H atoms were introduced in calculated, ideal positions and refined as riding on their parent C atom. Cell parameters were refined using up to 8192 reflections. A full sphere of data (1850 frames) was collected using the ω-scan method (0.3° frame width). The first 50 frames were remeasured at the end of data collection to monitor instrument and crystal stability (maximum correction on I was <1%). Absorption corrections by integration were applied based on measured indexed crystal faces.

For **3**·2Bu^tOH, an initial survey of reciprocal space revealed a set of reflections with an orthorhombic lattice. Analysis of the full data set revealed that the space group was $Pca2_1$. The asymmetric unit consists of a complete Mn_{12} cluster and two Bu^tOH molecules. There is one mode of disorder involving three O atoms: (a) O29/O44 are part of bridging carboxylate and O50 is water, and (b) O29 is water and O44/O50 are part of a carboxylate (see Supporting Information, Figure S2); the two possibilities refine to a 80:20 ratio, respectively. H atoms on atoms O33, O37, and O48 were obtained from a difference Fourier map and refined freely, while those on O44, O49, and O50 were calculated in idealized positions. A total of 1620 parameters were refined in the final cycle of refinement using 31760 reflections with $I > 2\sigma(I)$ to yield R_1 and wR_2 of 3.18 and 7.78%, respectively.

For **4**, an initial survey of reciprocal space revealed a set of reflections with a monoclinic lattice. Analysis of the full data set revealed that the space group was $P2_1/c$. The crystals were twinned by a pseudo 2-fold rotation axis along the *a*-axis (twin 1 0 0 0 −1 0 0 0 −1; basf = 0.355). The asymmetric unit consists of a complete Mn_{12} cluster. H atoms on the *n*-pentanol O atoms could not be observed, and they were thus placed in calculated positions and refined as riding on their parent O atoms. A total of 1581 parameters were included in the final refinement cycle using 26543 reflections with $I > 2\sigma(I)$ to yield R_1 and wR_2 of 8.01 and 17.58%, respectively.

The crystallographic data and structure refinement details for the two compounds are collected in Table 1.

AC Magnetic Susceptibility Studies. Variable-temperature AC magnetic susceptibility data were collected on a Quantum Design MPMS-XL SQUID magnetometer in the 1.8−15 K range using a 3.5 Oe AC field oscillating at frequencies up to

(17) (a) Eppley, H. J.; Tsai, H.-L.; de Vries, N.; Folting, K.; Christou, G.; Hendrickson, D. N. *J. Am. Chem. Soc.* **1995**, *117*, 301. (b) Tsai, H.-L.; Hendrickson, D. N.; Eppley, H. J.; de Vries, N.; Folting, K.; Christou, G. *J. Chem. Soc., Chem. Commun.* **1994**, 1745. (c) Eppley, H. J.; Tsai, H.-L.; de Vries, N.; Folting, K.; Christou, G.; Hendrickson, D. N. *J. Am. Chem. Soc.* **1995**, *117*, 301.

(18) (a) Soler, M.; Chandra, S. K.; Ruiz, D.; Huffman, J. C.; Hendrickson, D. N.; Christou, G. *Polyhedron* **2001**, *20*, 1279. (b) Soler, M.; Wernsdorfer, W.; Abboud, K. A.; Huffman, J. C.; Davidson, E. R.; Hendrickson, D. N.; Christou, G. *J. Am. Chem. Soc.* **2003**, *135*, 3576. (c) Soler, M.; Wernsdorfer, W.; Abboud, K. A.; Hendrickson, D. N.; Christou, G. *Polyhedron* **2003**, *22*, 1777.

(19) Bagai, R.; Christou, G. *Inorg. Chem.* **2007**, *46*, 10810.

(20) (a) Artus, P.; Boskovic, C.; Yoo, Y.; Streib, W. E.; Brunel, L.-C.; Hendrickson, D. N.; Christou, G. *Inorg. Chem.* **2001**, *40*, 4199. (b) Chakov, N. E.; Zakharov, L. N.; Rheingold, A. L.; Abboud, K. A.; Christou, G. *Inorg. Chem.* **2005**, *44*, 4555.

(21) (a) Wernsdorfer, W.; Murugesu, M.; Christou, G. *Phys. Rev. Lett.* **2006**, *96*, 057208. (b) Harter, A. G.; Lampropoulos, C.; Murugesu, M.; Kuhns, P.; Reyes, A.; Christou, G.; Dalal, N. S. *Polyhedron* **2007**, *26*, 2320. (c) Wernsdorfer, W.; Murugesu, M.; Tasiopoulos, A. J.; Christou, G. *Phys. Rev. B* **2005**, *72*, 212406. (d) Hill, S.; Anderson, N.; Wilson, A.; Takahashi, S.; Petukhov, K.; Chakov, N. E.; Murugesu, M.; North, J. M.; del Barco, E.; Kent, A. D.; Dalal, N. S.; Christou, G. *Polyhedron* **2005**, *24*, 2284. (e) Lampropoulos, C.; Lawrence, J.; Harter, A. G.; Wernsdorfer, W.; Hill, S. O.; Dalal, N. S.; Abboud, K. A.; Christou, G. *Inorg. Chem.* **2009**, in preparation. (f) Barra, A.-L.; Caneschi, A.; Cornia, A.; Gatteschi, D.; Gorini, L.; Heiniger, L.-P.; Sessoli, R.; Sorace, L. *J. Am. Chem. Soc.* **2007**, *129*, 10754.

(22) Lis, T. *Acta Crystallogr., Sect. B* **1980**, *B36*, 2042.

Table 1. Crystal Data and Structure Refinement Parameters for Complexes **3** and **4**

parameter	**3**	**4**
formula[a]	$C_{108}H_{212}Mn_{12}O_{49.2}$	$C_{116}H_{224}Mn_{12}O_{48}$
fw, g/mol[a]	2955.24	3046.23
space group	*Pca*2(1)	*P*2(1)/*c*
a, Å	23.601(2)	29.810(5)
b, Å	20.4694(18)	25.142(5)
c, Å	29.917(3)	20.156(4)
α, deg	90	90
β, deg	90	90.097(3)
γ, deg	90	90
V, Å^3	14453(2)	15107(5)
Z	4	4
T, K	173(2)	100(2)
radiation, Å[b]	0.71073	0.71073
ρ_{calc}, mg/m^3	1.358	1.339
μ, mm^{-1}	1.085	1.040
R1[c,d]	0.0318	0.0801
wR2[e]	0.0778	0.1758

[a] Including solvate molecules. [b] Graphite monochromator. [c] $I > 2\sigma(I)$. [d] $R1 = 100\sum||F_o| - |F_c||/\sum|F_o|$. [e] $wR2 = 100[\sum w(F_o^2 - F_c^2)^2/\sum w(F_o^2)^2]^{1/2}$, $w = 1/[\sigma^2(F_o^2) + [(ap)^2 + bp]$, where $p = [\max(F_o^2, O) + 2F_c^2]/3$.

1500 Hz. Pascal's constants were used to estimate the diamagnetic corrections, which were subtracted from the experimental susceptibilities to give the molar paramagnetic susceptibilities (χ_M'). To measure the molar AC susceptibility of samples that had been kept wet with mother liquor, crystals were removed from the mother liquor, dried well on absorbent tissue paper, transferred to an analytical balance for accurate weighing, and then carefully embedded in eicosane within a gelatin capsule for magnetism measurements. The whole procedure took only a few minutes, and it was assumed that it ensured retention of the crystallographic formulations of **3**·2Bu^{t}OH and **4**, so the corresponding molecular weights were employed for calculation of molar amounts.

HFEPR Spectroscopy. HFEPR measurements were carried out on single-crystals of **3**·2Bu^{t}OH and **4** at various discrete frequencies in the 200 to 402 GHz range. An oversized cylindrical resonator was employed to provide enhanced sensitivity, and a Millimeter-wave Vector Network Analyzer (MVNA) served as a superheterodyne spectrometer (described elsewhere).[23,24] A 7 T horizontal-bore superconducting magnet associated with a Quantum Design PPMS system enabled in situ rotation of the cavity relative to the applied field, allowing field-orientation-dependent studies about a single-axis; a time-consuming option to rotate the cavity about a second orthogonal axis was not employed for these investigations. Sample alignment was instead achieved by first aligning the needle-shaped crystals by eye, then performing in situ single-axis rotation studies to locate extrema (easy/hard directions) among plots of the angle-dependent EPR peak positions. Once aligned, measurements were performed as a function of frequency and temperature so as to provide data sets which maximally constrain the ZFS parameters. The cavity/sample temperature was regulated by means of the sophisticated flow cryostat integrated into the PPMS system.

The HFEPR data were obtained with the magnetic field approximately parallel to the easy axis of the crystal. Since only a single-axis rotation capability was employed, perfect easy-axis alignment is not guaranteed. Consequently, the obtained *g* values are not reliable. However, extrapolation of simulations to zero-field enables very tight constraints on the axial ZFS parameters *D* and B_4^0 (vide infra), which ultimately determine the barrier to magnetization relaxation in a SMM; we note that the high-frequency (> 100 GHz) easy-axis spectra for Mn_{12} are completely insensitive to the transverse ZFS parameters. Prior to measurement, crystals of **3**·2Bu^{t}OH and **4** were quickly transferred from their mother liquor and coated in silicone grease for protection. The samples were also initially cooled under He helium gas, with a total transfer time from the mother liquor to the cryostat of ~5 min.

Other Studies. Infrared spectra were recorded in the solid state (KBr pellets) on a Nicolet Nexus 670 FTIR spectrometer in the 400−4000 cm^{-1} range. Elemental analyses (C, H, and N) were performed by the in-house facilities of the University of Florida Chemistry Department.

Results and Discussion

Synthesis. The efficient carboxylate-substitution methodology that we previously developed for the replacement of all acetate groups of readily available $[Mn_{12}O_{12}(O_2CMe)_{16}(H_2O)_4]\cdot 2MeCO_2H\cdot 4H_2O$ (**1**, Mn_{12}−Ac) with essentially any other carboxylate of choice has opened up access to a large family of Mn_{12} derivatives.[15i,25,26] This has made possible the controlled modification of various properties of interest, such as solubility, redox potentials, crystallinity, and the presence of deuterated or element-labeled (e.g., F) ligands for specific spectroscopic studies. In the present work, this has been extended to include modification of the neutral ligands on the Mn_{12} cluster by incorporation of alcohols in place of the bound H_2O; previous work along these lines has been limited to MeOH,[21,27] but in the present work higher alcohols have been employed together with bulky *t*-butylacetate ligands in a direct one-step dual-substitution reaction starting with complex **1**. The procedure to **3** involves the heating of a solution **1** and an excess of Bu^{t}CH$_2$CO$_2$H in Bu^{t}OH. Both these conditions are necessary to ensure complete substitution, otherwise mixed-carboxylate species will be obtained. The preparation of **3** is summarized in eq 1.

$$[Mn_{12}O_{12}(O_2CMe)_{16}(H_2O)_4] + 16Bu^tCH_2CO_2H + Bu^tOH \rightarrow [Mn_{12}O_{12}(O_2CCH_2Bu^t)_{16}(Bu^tOH)(H_2O)_3] + 16MeCO_2H + H_2O \quad (1)$$

Complex **4** was obtained in a similar fashion using *n*-pentanol, and its synthesis is summarized in eq 2. The major difference between **3** versus **4** is the incorporation of only one alcohol molecule

$$[Mn_{12}O_{12}(O_2CMe)_{16}(H_2O)_4] + 16Bu^tCH_2CO_2H + 4C_5H_{11}OH \rightarrow [Mn_{12}O_{12}(O_2CCH_2Bu^t)_{16}(C_5H_{11}OH)_4] + 16MeCO_2H + 4H_2O \quad (2)$$

(23) Mola, M.; Hill, S.; Goy, P.; Gross, M. *Rev. Sci. Instrum.* **2000**, *71*, 186.
(24) Takahashi, S.; Hill, S. *Rev. Sci. Instrum.* **2005**, *76*, 023114.
(25) (a) Soler, M.; Artus, P.; Folting, K.; Huffman, J. C.; Hendrickson, D. N.; Christou, G. *Inorg. Chem.* **2001**, *40*, 4902. (b) Chakov, N. E.; Abboud, K. A.; Zakharov, L. N.; Rheingold, A. L.; Hendrickson, D. N.; Christou, G. *Polyhedron* **2003**, *22*, 1759. (c) Brockman, J. T.; Abboud, K. A.; Hendrickson, D. N.; Christou, G. *Polyhedron* **2003**, *22*, 1765. (d) Soler, M.; Wernsdorfer, W.; Sun, Z.; Ruiz, D.; Huffman, J. C.; Hendrickson, D. N.; Christou, G. *Polyhedron* **2003**, *22*, 1783.
(26) (a) Soler, M.; Wernsdorfer, W.; Abboud, K. A.; Huffman, J. C.; Davidson, E. R.; Hendrickson, D. N.; Christou, G. *J. Am. Chem. Soc.* **2003**, *125*, 3576. (b) Chakov, N. E.; Soler, M.; Wernsdorfer, W.; Abboud, K. A.; Christou, G. *Inorg. Chem.* **2005**, *44*, 53041. (c) Chakov, N. E.; Lee, S. C.; Harter, A. G.; Kuhns, P. L.; Reyes, A. P.; Hill, S. O.; Dalal, N. S.; Wernsdorfer, W.; Abboud, K. A.; Christou, G. *J. Am. Chem. Soc.* **2006**, *128*, 6975.
(27) Bian, G. Q.; Kuroda-Sowa, T.; Gunjima, N.; Maekawa, M.; Munakata, M. *Inorg. Chem. Commun.* **2005**, *8*, 208.

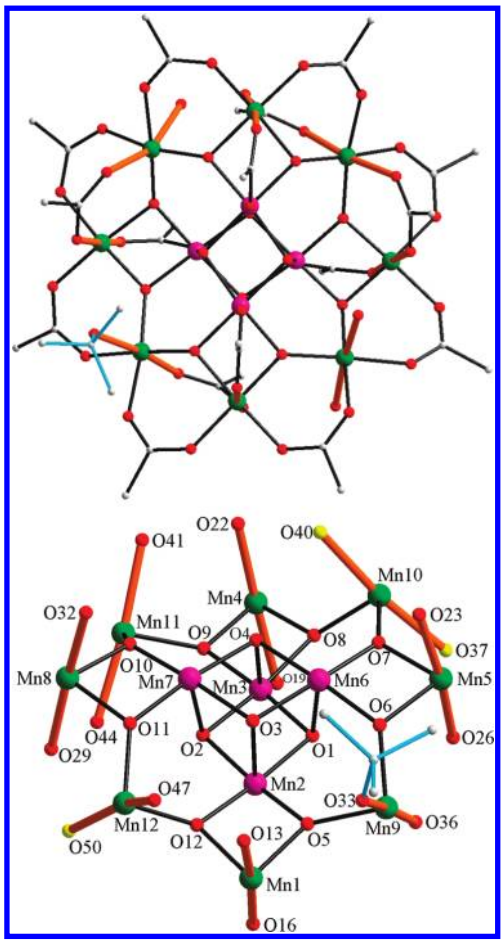

Figure 1. PovRay representations of complex **3** (top) and its labeled core (bottom). Hydrogen atoms and carboxylate Me carbon atoms have been omitted for clarity. The Mn^{III} JT elongation axes are denoted as thick orange bonds; the Bu^tOH ligand is denoted in sky-blue. Color code: Mn^{IV} purple; Mn^{III} green; O red; H_2O yellow; C gray.

in the former (vide infra), which can be assigned to the steric congestion arising from the bulk of both the alcohol and the $Bu^tCH_2CO_2^-$ groups.

Description of Structures. Complex **3**·2Bu^tOH crystallizes in the orthorhombic space group $Pca2_1$. A top-view of the structure and its labeled core are shown in Figure 1. Selected interatomic distances and angles are listed in Table 2. The overall structure of $[Mn_{12}O_{12}(O_2CCH_2Bu^t)_{16}(Bu^tOH)(H_2O)_3]$ (**3**) is very similar to previously characterized members of the $[Mn_{12}O_{12}(O_2CR)_{16}(solv)_4]$ (solv = H_2O, MeOH) family such as $[Mn_{12}O_{12}(O_2CCH_2Bu^t)_{16}(MeOH)_4]$ (**2**).[21e,25−27] There is a central $[Mn^{IV}{}_4O_4]^{8+}$ cubane bridged by eight additional μ_3-O^{2-} ions to a surrounding nonplanar ring of eight Mn^{III} ions.[14] Peripheral ligation is provided by sixteen η^1:η^1-μ-$O_2CCH_2Bu^t$ anions and four terminal solvent molecules. At this point, a significant difference between **2** and **3** becomes evident in both the nature of the bound solvent molecules and their positioning about the Mn_{12} core: the former contains four terminal MeOH groups that are symmetrically disposed in a 1:1:1:1 fashion (i.e., one MeOH on each of four alternating Mn^{III} atoms) about the $[Mn_{12}O_{12}]$ core to give S_4 point group symmetry, and this results in the carboxylate ligands also being symmetrically disposed. In contrast, **3** contains only one Bu^tOH (O33) and three H_2O molecules (O37, O40, and O50) that, in addition, are disposed in an asymmetric 2:1:1 fashion, the Bu^tOH (bound to Mn9) being the central ligand (i.e., $(H_2O)_2$:Bu^tOH:H_2O), to give a cluster with no virtual symmetry (point group C_1). We rationalize this low content of bound Bu^tOH and the asymmetric solvent disposition as reflecting the impossibility, because of steric congestion, of accommodating 16 bulky $Bu^tCH_2CO_2^-$ and more than one Bu^tOH around the $[Mn_{12}O_{12}]$ core. Even to accommodate one Bu^tOH, the carboxylates arrange in an asymmetric fashion to open up sufficient space. This also causes the three bound water molecules to be surrounded to different degrees by the carboxylate $-CH_2Bu^t$ groups (Supporting Information, Figure S1): water O50 is completely enveloped and almost not visible; water O40 is more exposed but still too buried to form H-bonds to lattice molecules; and water O37 is the most exposed, not sufficient to accommodate a Bu^tOH in its place but enough to form H-bonds to the two lattice Bu^tOH molecules, one strong (O37H···O48 = 2.715 Å) and one weak (O37···HO49 = 3.15 Å).[28]

All the Mn ions are six-coordinate with near-octahedral geometry. The Mn oxidation states were as expected for a Mn_{12} cluster,[14] and they were confirmed by bond

Table 2. Selected Core Interatomic Distances (Å) for Complex **3**

Mn1···Mn2	2.777(1)	Mn3···Mn6	2.828(1)
Mn2···Mn3	2.900(1)	Mn3···Mn7	2.855(1)
Mn2···Mn6	2.818(1)	Mn5···Mn6	2.770(1)
Mn2···Mn7	2.844(1)	Mn6···Mn7	2.931(1)
Mn3···Mn4	2.771(1)	Mn7···Mn8	2.768(1)
Mn1−O5	1.888(1)	Mn7−O11	1.863(1)
Mn1−O12	1.919(1)	Mn7−O10	1.873(1)
Mn1−O14	1.948(2)	Mn7−O2	1.914(1)
Mn1−O15	1.958(2)	Mn7−O28	1.918(2)
Mn1−O13	2.156(2)	Mn7−O4	1.918(1)
Mn1−O16	2.204(2)	Mn7−O3	1.927(1)
Mn2−O12	1.862(1)	Mn8−O10	1.900(1)
Mn2−O5	1.865(1)	Mn8−O11	1.925(1)
Mn2−O2	1.900(1)	Mn8−O30	1.954(2)
Mn2−O1	1.907(1)	Mn8−O31	1.955(2)
Mn2−O3	1.917(1)	Mn8−O29	2.097(3)
Mn2−O17	1.919(2)	Mn8−O32	2.166(2)
Mn3−O9	1.840(1)	Mn9−O5	1.879(1)
Mn3−O8	1.886(1)	Mn9−O6	1.901(1)
Mn3−O1	1.909(1)	Mn9−O34	1.951(2)
Mn3−O4	1.917(1)	Mn9−O35	1.958(1)
Mn3−O2	1.920(1)	Mn9−O36	2.124(2)
Mn3−O18	1.922(1)	Mn9−O33	2.302(2)
Mn4−O9	1.875(1)	Mn10−O7	1.870(1)
Mn4−O8	1.922(1)	Mn10−O8	1.898(1)
Mn4−O21	1.938(1)	Mn10−O38	1.951(1)
Mn4−O20	1.947(1)	Mn10−O39	1.954(1)
Mn4−O22	2.160(1)	Mn10−O37	2.222(2)
Mn4−O19	2.253(2)	Mn10−O40	2.241(2)
Mn5−O7	1.882(1)	Mn11−O9	1.887(1)
Mn5−O6	1.912(1)	Mn11−O10	1.934(2)
Mn5−O24	1.941(1)	Mn11−O43	1.945(2)
Mn5−O25	1.943(1)	Mn11−O42	1.976(2)
Mn5−O26	2.189(2)	Mn11−O44	2.127(2)
Mn5−O23	2.229(1)	Mn11−O41	2.164(2)
Mn6−O7	1.860(1)	Mn12−O12	1.864(1)
Mn6−O6	1.881(1)	Mn12−O11	1.878(1)
Mn6−O3	1.900(1)	Mn12−O45	1.942(2)
Mn6−O1	1.903(1)	Mn12−O46	1.952(2)
Mn6−O27	1.923(1)	Mn12−O47	2.066(2)
Mn6−O4	1.931(1)	Mn12−O50	2.324(2)

(28) (a) Bartha, F.; Kapuy, O.; Kozmutza, C.; Van Alsenoy, C. *THEOCHEM* **2003**, *666*−*667*, 117. (b) Kozmutza, C.; Varga, I.; Udvardi, L. *THEOCHEM* **2003**, *666*−*667*, 95. (c) Hibbert, F.; Emsley, J. *Adv. Phys. Org. Chem.* **1990**, *26*, 255. (d) Emsley, J. *Chem. Soc. Rev.* **1980**, *9*, 91.

valence sum (BVS) calculations (Supporting Information, Table S1).[29] The Mn^{III} atoms are Jahn−Teller (JT) distorted, exhibiting axially elongated bonds ~0.1−0.2 Å longer than the equatorial bonds. These JT elongation axes are all in what has come to be known as the "normal" orientation, that is, approximately parallel to each other and perpendicular to the plane of this disk-like molecule, thus avoiding the $Mn-O^{2-}$ bonds. Complex **3** is thus a "normal" JT isomer, where "JT isomerism" is defined as the ability of a molecule to exist in different isomeric forms differing in the relative orientation of one or more JT axes. The rarer "abnormal" JT isomers of the Mn_{12} family are the handful of examples that have one (or more) JT axes oriented approximately in the plane of the molecule and pointing toward an O^{2-} ion.[14,30−32] Finally, there are no significant intermolecular interactions because the lattice Bu^tOH molecules form H-bonds only to one Mn_{12} molecule and do not also H-bond to a neighboring one.

Complex **4** crystallizes in the monoclinic space group $P2_1/c$. A top-view of the structure and its labeled core are shown in Figure 2. Selected interatomic distances and angles are listed in Table 3. The overall structure of **4** is again as expected for an Mn_{12} complex. The $[Mn_{12}O_{12}]$ core is as for **3**, and the peripheral ligation is again by 16 carboxylates and 4 solvent molecules, but now there is a more symmetric distribution of the $Bu^tCH_2CO_2^-$ and *n*-pentanol ligands, with the extended structure of the latter clearly precluding the steric problems encountered in **3** with the bulky Bu^tOH groups. In fact, complex **4** contains four *n*-pentanol ligands (and thus no water ligands) arranged in 2:2 fashion (i.e., two each on Mn^{III} atoms Mn9 and Mn11) to give a complex of virtual D_2 point group symmetry, as seen previously for the benzoate complex $[Mn_{12}O_{12}(O_2CPh)_{16}(H_2O)_4]$.[2]

The outer Mn^{III} atoms again have all their JT elongation axes oriented in the "normal" direction avoiding the $Mn-O^{2-}$ bonds. Relevant to the HFEPR studies to be described below is the presence of two orientations of Mn_{12} molecules in the unit cell, as shown in the packing diagram in Supporting Information, Figure S3. The angle between the two orientations is 55° (measured as the angle between the Mn_{12} least-squares plane of each molecule); the two orientations are related by a crystallographic screw axis. There are no significant intermolecular interactions between adjacent Mn_{12} molecules.

Also of relevance to the magnetic and HFEPR studies and discussion to follow is a comparison of the structures of the $[Mn_{12}O_{12}]$ cores of **3** and **4**. The low symmetry in the ligand disposition in **3** and the steric congestion from the bulky Bu^tOH and $Bu^tCH_2CO_2^-$ groups leads in turn

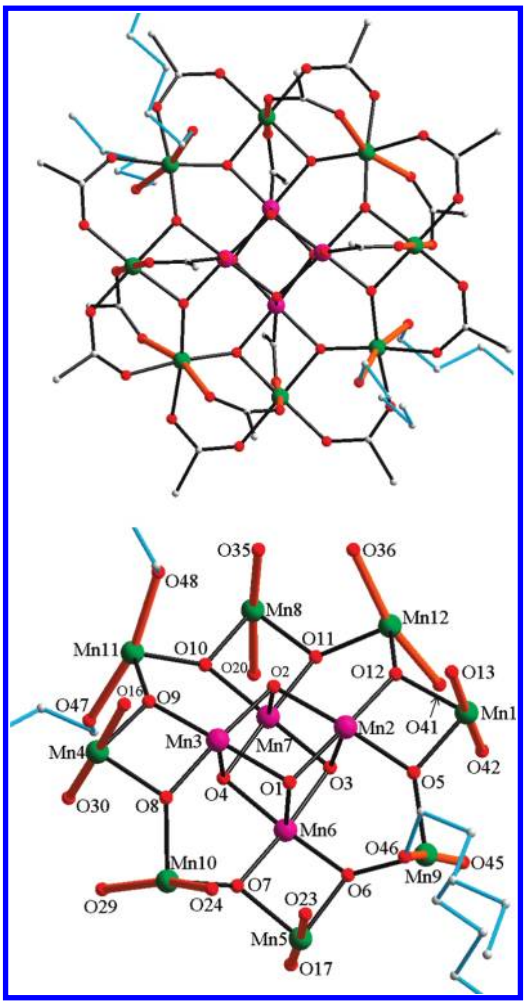

Figure 2. PovRay representations of complex **4** (top) and its labeled core (bottom). Hydrogen atoms and carboxylate Me carbon atoms have been omitted for clarity. The Mn^{III} JT elongation axes are denoted as thick orange bonds; the *n*-propanol ligands are denoted in sky-blue and truncated in places. Color code: Mn^{IV} purple; Mn^{III} green; O red; C gray.

to a significant distortion of its $[Mn_{12}O_{12}]$ core compared with that of **4**, which is symmetric. This is clearly apparent in Figure 3. When viewed from the side, the Mn_{12} atoms separate into three layers, with four alternating Mn^{III} atoms occupying the middle layer. Figure 3 (bottom) shows the complete $[Mn_{12}O_{48}]$ unit of **4** viewed from the side along the least-squares plane of the eight Mn atoms of the top and bottom layers; the four Mn atoms of the middle layer lie in this plane. In contrast, the core of **3** in Figure 3 (top) is clearly distorted with the atoms of the middle layer much displaced from the least-squares plane, by 0.034, 0.176, 0.458, and 0.494 Å for Mn12, Mn9, Mn10, and Mn11, respectively. This also leads to a significant tilting of these Mn^{III} JT axes, which are emphasized as thicker orange bonds, in a random fashion. This (i) removes their near-symmetric arrangement about the *z*-axis (as found in **4**), and thus **3** is expected to have significant transverse anisotropy in the *xy*-plane, and (ii) decreases the average angle between them and the *xy*-plane, thus decreasing their projection along the *z*-axis, which is expected to thus decrease the axial anisotropy parameter, *D*. As will be seen below, these are consistent with the observed properties of **3**.

(29) (a) Brown, I. D.; Altermatt, D. *Acta Crystallogr.* **1985**, *B41*, 244. (b) Palenik, G. J. *Inorg. Chem.* **1997**, *36*, 4888. (c) Palenik, G. J. *Inorg. Chem.* **1997**, *36*, 122.

(30) (a) Sun, Z.; Ruiz, D.; Dilley, N. R.; Soler, M.; Ribas, J.; Folting, K.; Maple, M. B.; Christou, G.; Hendrickson, D. N. *Chem. Commun.* **1999**, 1973. (b) Aubin, S. M. J.; Sun, Z.; Eppley, H. J.; Rumberger, E. M.; Guzei, I. A.; Folting, P. K.; Gantzel, P. K.; Rheingold, A. L.; Christou, G.; Hendrickson, D. N. *Polyhedron* **2001**, *20*, 1139.

(31) Aubin, S. M. J.; Sun, Z.; Eppley, H. J.; Rumberger, E. M.; Guzei, I. A.; Folting, K.; Gantzel, P. K.; Rheingold, A. L.; Christou, G.; Hendrickson, D. N. *Inorg. Chem.* **2001**, *40*, 2127.

(32) Soler, M.; Wernsdorfer, W.; Sun, Z.; Huffman, J. C.; Hendrickson, D. N.; Christou, G. *Chem. Commun.* **2003**, 2672.

Table 3. Selected Core Interatomic Distances (Å) for **4**

Mn1···Mn2	2.788(1)	Mn3···Mn6	2.820(1)
Mn2···Mn3	2.940(1)	Mn3···Mn7	2.831(2)
Mn2···Mn6	2.837(1)	Mn5···Mn6	2.766(1)
Mn2···Mn7	2.822(1)	Mn6···Mn7	2.923(1)
Mn3···Mn4	2.781(1)	Mn7···Mn8	2.775(1)
Mn1−O12	1.895(5)	Mn7−O11	1.866(6)
Mn1−O5	1.902(6)	Mn7−O2	1.886(6)
Mn1−O40	1.935(6)	Mn7−O10	1.888(6)
Mn1−O43	1.949(6)	Mn7−O3	1.895(5)
Mn1−O42	2.165(6)	Mn7−O19	1.907(7)
Mn1−O13	2.199(6)	Mn7−O4	1.917(6)
Mn2−O12	1.849(5)	Mn8−O11	1.887(6)
Mn2−O5	1.875(6)	Mn8−O10	1.908(6)
Mn2−O1	1.917(5)	Mn8−O37	1.947(6)
Mn2−O14	1.920(6)	Mn8−O34	1.951(7)
Mn2−O2	1.924(6)	Mn8−O35	2.170(8)
Mn2−O3	1.926(5)	Mn8−O20	2.217(7)
Mn3−O9	1.871(6)	Mn9−O5	1.887(6)
Mn3−O8	1.871(6)	Mn9−O6	1.914(6)
Mn3−O4	1.897(6)	Mn9−O21	1.953(6)
Mn3−O15	1.906(7)	Mn9−O44	1.972(6)
Mn3−O2	1.923(6)	Mn9−O45	2.179(6)
Mn3−O1	1.926(5)	Mn9−O46	2.185(6)
Mn4−O8	1.890(6)	Mn10−O7	1.884(6)
Mn4−O9	1.909(6)	Mn10−O8	1.894(6)
Mn4−O31	1.943(7)	Mn10−O26	1.971(6)
Mn4−O28	1.955(7)	Mn10−O27	1.974(6)
Mn4−O30	2.152(8)	Mn10−O24	2.147(6)
Mn4−O16	2.193(8)	Mn10−O29	2.211(7)
Mn5−O6	1.897(6)	Mn11−O9	1.884(6)
Mn5−O7	1.903(5)	Mn11−O10	1.885(6)
Mn5−O25	1.925(6)	Mn11−O33	1.949(8)
Mn5−O22	1.954(6)	Mn11−O32	1.955(8)
Mn5−O23	2.170(6)	Mn11−O47	2.163(8)
Mn5−O17	2.202(6)	Mn11−O48	2.192(9)
Mn6−O6	1.856(5)	Mn12−O11	1.896(6)
Mn6−O7	1.883(6)	Mn12−O12	1.905(6)
Mn6−O1	1.891(5)	Mn12−O38	1.970(6)
Mn6−O4	1.902(6)	Mn12−O39	1.974(6)
Mn6−O18	1.905(6)	Mn12−O41	2.137(7)
Mn6−O3	1.918(5)	Mn12−O36	2.163(7)

AC Magnetic Susceptibility Studies on Complexes 3 and 4. AC susceptibility data were collected on polycrystalline samples of **3**·2Bu^{t}OH and **4** in the 1.8−15 K range in a 3.5 G AC field oscillating at eight frequencies (υ) in the 5−1500 Hz range. In an AC susceptibility experiment, the magnetization vector of the sample oscillates with the AC field, and there is no out-of-phase (χ_M'') AC signal unless the temperature is lowered to a value at which the barrier to magnetization relaxation is comparable to the thermal energy.[16] A frequency-dependent χ_M'' signal is then observed, along with the concomitant frequency-dependent decrease in the in-phase (χ_M') signal. A frequency-dependent χ_M'' signal is a necessary but not sufficient[33] indicator of the superparamagnet-like properties of a single-molecule magnet (SMM). The value of $\chi_M'T$ at the lowest temperatures is also especially useful, providing information about the ground state spin of a molecule.[10d,34]

In Figure 4 are shown the in-phase (χ_M', plotted as $\chi_M'T$) and out-of-phase (χ_M'') AC susceptibility signals for a sample of **3**·2Bu^{t}OH. Extrapolation of the in-phase data to 0 K from above ~9 K gives $\chi_M'T \sim 56$ cm^3 K mol^{-1}, indicating an $S = 10$ ground state with $g \sim 2.0$, which is the expected ground state spin of a Mn_{12} complex. At lower temperatures, there is a frequency-dependent decrease in $\chi_M'T$ and a concomitant increase in χ_M'', indicating **3**·2Bu^{t}OH to be an SMM, as indeed expected for a Mn_{12} complex.[14] At lower temperatures, a second feature in either $\chi_M'T$ or χ_M'' is not detectable, indicating the absence of any faster-relaxing Mn_{12} species in the sample. Therefore, the phenomenon of JT isomerism was not observed for **3**·2Bu^{t}OH.

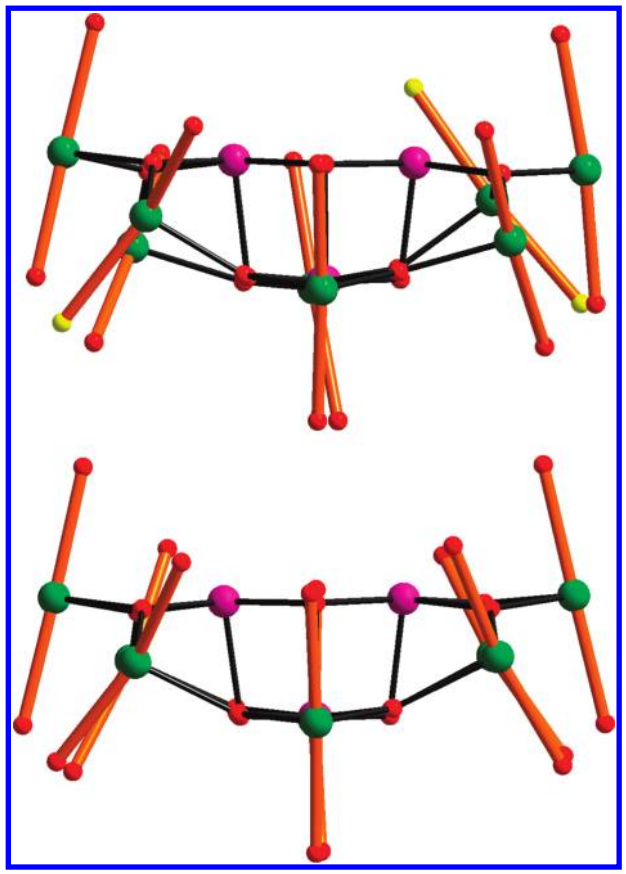

Figure 3. [$Mn_{12}O_{48}$] cores of complexes **3** (top) and **4** (bottom), viewed approximately along the least-squares plane of the eight Mn atoms of the top and bottom layers, emphasizing the distorted nature of **3**. Color code: Mn^{IV} purple, Mn^{III} green, O red, H_2O yellow, Jahn-Teller elongation axes brown.

The corresponding in-phase ($\chi_M'T$) and out-of-phase (χ_M'') AC susceptibility signals for **4** are shown in Figure 5. The overall behavior of **4** is very similar to that of **3**·2Bu^{t}OH, with again no sign of a second feature in either $\chi_M'T$ or χ_M'' at lower temperatures assignable to a faster-relaxing "abnormal" JT isomer in the sample, and extrapolation of the in-phase data to 0 K from above 9 K again giving ~55 cm^3 K mol^{-1} indicative of an $S = 10$ ground state with $g \sim 2.0$. There are, however, a few differences between **3**·2Bu^{t}OH and **4** deserving special mention. The temperatures at which a frequency-dependent decrease in $\chi_M'T$ and a concomitant increase in χ_M'' first appear at a given frequency differ by ~1 K for the two compounds, with those for **4** being the higher. This is seen also in the χ_M'' peak maximum temperature at $\upsilon = 1500$ Hz, which is 7.7 K for **4** versus 6.6 K for **3**·2Bu^{t}OH. Accordingly, the peaks for **4** at other frequencies appear at correspondingly higher temperatures than

(33) Chakov, N. E.; Wernsdorfer, W.; Abboud, K. A.; Christou, G. *Inorg. Chem.* **2004**, *43*, 5919.

(34) (a) Soler, M.; Wernsdorfer, W.; Folting, K.; Pink, M.; Christou, G. *J. Am. Chem. Soc.* **2004**, *126*, 2156. (b) Sañudo, E. C.; Wernsdorfer, W.; Abboud, K. A.; Christou, G. *Inorg. Chem.* **2004**, *43*, 4137. (c) Brechin, E. B.; Sanudo, E. C.; Wernsdorfer, W.; Boskovic, C.; Yoo, J.; Hendrickson, D. N.; Yamaguchi, A.; Ishimoto, H.; Concolino, T. E.; Rheingold, A. L.; Christou, G. *Inorg. Chem.* **2005**, *44*, 502.

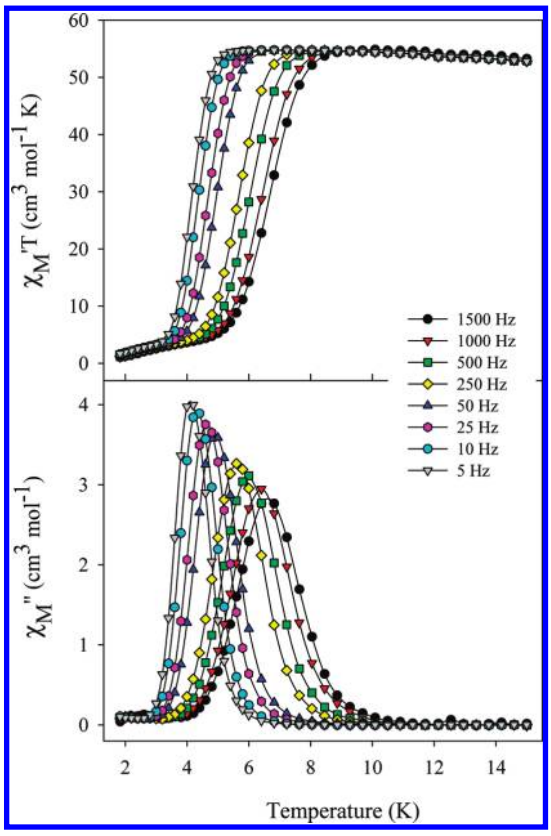

Figure 4. Plot of the in-phase ($\chi_M'T$) and out-of-phase (χ_M'') AC susceptibility signals versus temperature for a polycrystalline sample of complex **3**·2Bu^{t}OH, freshly removed from mother liquor, at the indicated oscillation frequencies.

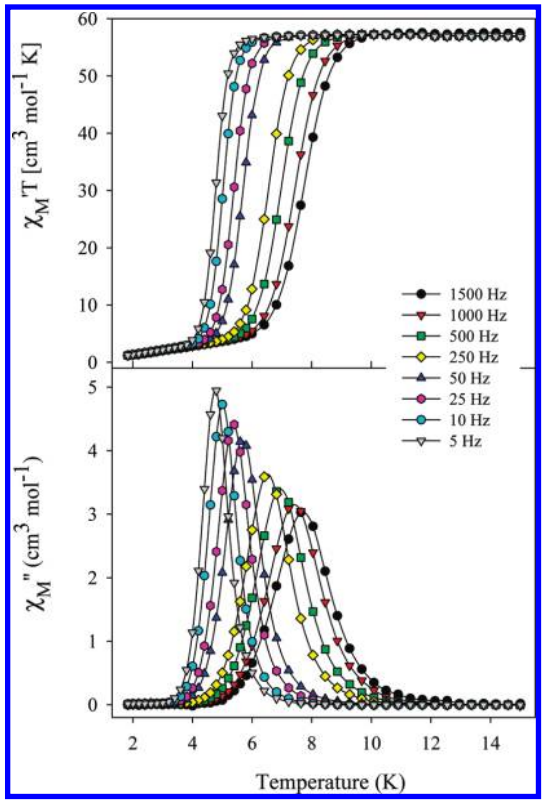

Figure 5. Plot of the in-phase ($\chi_M'T$) and out-of-phase (χ_M'') AC susceptibility signals versus temperature for complex **4**, freshly removed from mother liquor, at the indicated oscillation frequencies.

for **3**·2Bu^{t}OH. These data indicate that the magnetization relaxation rate of **3**·2Bu^{t}OH is faster than that of **4** at a given temperature. To probe this further, we carried out a quantitative analysis of the relaxation kinetics using the AC data.

The χ_M'' versus T plots were used as a source of data with which to determine the effective kinetic energy barrier (U_{eff}) to magnetization relaxation.[35] At a given oscillation frequency (υ), the position of the χ_M'' peak maximum is the temperature at which the angular frequency ($\omega = 2\pi\upsilon$) of the oscillating field equals the relaxation rate ($1/\tau$, where τ is the relaxation time) at which a molecule relaxes between the halves of the double-well potential energy plot. The relaxation rates at a given temperature can thus be obtained from $\omega = 1/\tau$ at the χ_M'' peak maxima, and each peak was fit to a Lorentzian function to obtain the temperature at the maximum accurately. The data for **3**·2Bu^{t}OH and **4** are plotted as $\ln(1/\tau)$ versus $1/T$ in Figure 6 (top and bottom, respectively), and the solid lines are the fits to the Arrhenius relationship of eqs 3a and 3b, the characteristic behavior of a thermally activated Orbach process; k is the Boltzmann constant

$$(1/\tau) = (1/\tau_0)\exp(-U_{eff}/kT) \quad (3a)$$

$$\ln(1/\tau) = \ln(1/\tau_0) - (U_{eff}/kT) \quad (3b)$$

and $1/\tau_0$ is the pre-exponential factor. The fit parameters were $U_{eff} = 62.6$ K and $\tau_0 = 9.1 \times 10^{-9}$ s ($1/\tau_0 = 1.1 \times 10^8$ s^{-1}) for **3**·2Bu^{t}OH, and $U_{eff} = 71.2$ K and $\tau_0 = 1.1 \times 10^{-8}$ s ($1/\tau_0 = 9.1 \times 10^7$ s^{-1}) for **4**. The faster magnetization relaxation rate of **3**·2Bu^{t}OH versus **4** at a particular temperature, as deduced above from Figures 4 and 5, can now be rationalized. On the basis of eq 3a, differing relaxation rates ($1/\tau$) at a given temperature could be due to differing pre-exponential factors $1/\tau_0$, barriers U_{eff}, or both. Comparison of the fit data for **3**·2Bu^{t}OH and **4** shows that (i) **4** has the smaller $1/\tau_0$ by about 17% (the $1/\tau_0$ ratio for **4**/**3** is 0.83); and (ii) **4** has the higher U_{eff} by about 14% (the U_{eff} ratio for **4**/**3** is 1.14). These differences in $1/\tau_0$ and U_{eff} both serve to yield a slower relaxation rate for **4** versus **3** at a given temperature.

In a recent publication,[36] we showed that the magnetization relaxation of Mn_{12} SMMs, and by implication many other SMMs as well, does not follow the simple Arrhenius law of eq 3b, even for data collected at < 1500 Hz, owing to contributions from relaxation pathways via excited S states with a larger thermal barrier but much faster spin reversal rates because of larger pre-exponential ($1/\tau_0$) factors. This is reflected in a slight curvature of $\ln(1/\tau)$ versus $1/T$ plots, such as those in Figure 6. We provided a double-exponential modification of the Arrhenius equation (eq 4) that we consider a superior means to obtain the true barrier U_1 (U_{eff}) of an SMM in its ground

$$(1/\tau) = (1/\tau_{01})\exp(-U_1/kT) + (1/\tau_{02})\exp(-U_2/kT) \quad (4)$$

(35) Novak, M. A.; Sessoli, R. In *Quantum Tunneling of Magnetization – QTM '94*; Gunther, L., Barbara, B., Eds.; Kluwer: Amsterdam, 1995; pp 171–188.

(36) Lampropoulos, C.; Hill, S.; Christou, G. *Chem. Phys. Chem.* **2009**, *10*, 2397.

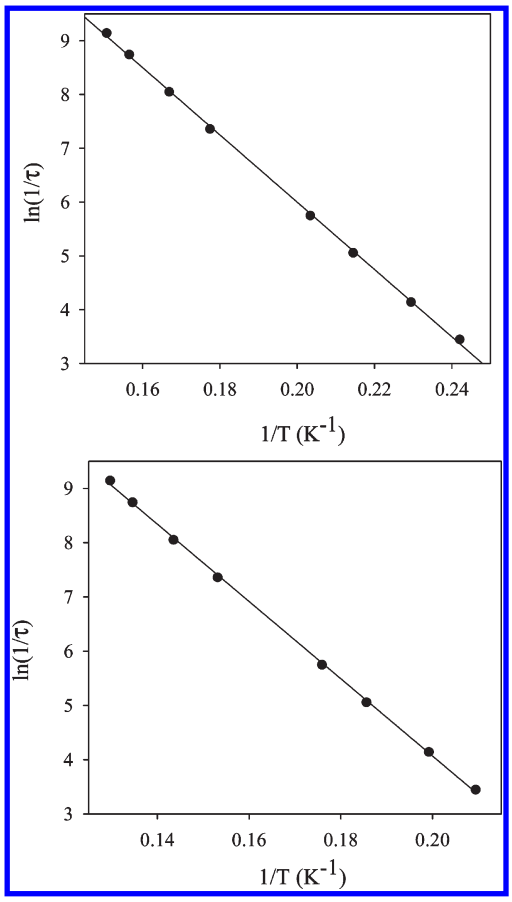

Figure 6. Plots of the natural logarithm of the magnetization relaxation rate versus $1/T$ for complexes **3**·2Bu^{t}OH (top) and **4** (bottom). The solid lines are fits to the Arrhenius equation of eq 3b. See the text for the fit parameters.

state by separating out the ground state relaxation pathway (first exponential term in eq 4) from those via excited states (second exponential term), where U_2 reflects the "average" excitation energy to a large group of excited S states that provide more efficient relaxation pathways.[36] Whereas eq 3b and its associated U_{eff} and $1/\tau_0$ are the appropriate ones to employ for comparing the overall AC behavior of Figures 4 and 5, the true kinetic barrier (U_{eff}) of the ground state of an SMM is given by U_1, and its associated pre-exponential is $1/\tau_{01}$. Fitting of AC susceptibility data to a single-exponential Arrhenius equation (i.e., eq 3) typically results in an overestimation of U_{eff}, whereas a fit to eq 4 gives a far more reliable value of U_{eff} (U_1) and $1/\tau_0$ ($1/\tau_{01}$).[36] Fits of the ln($1/\tau$) versus $1/T$ plots of Figure 6 to eq 4 gave fit parameters U_1 = 54.8(17) K, $\tau_{01} = 3.8(18) \times 10^{-7}$ s, U_2 = 82(5) K, $\tau_{02} = 5.4(30) \times 10^{-9}$ s for **3**·2Bu^{t}OH, and U_1 = 67.9(9) K, $\tau_{01} = 1.3(2) \times 10^{-7}$ s, U_2 = 123(18) K, $\tau_{02} = 3(2) \times 10^{-10}$ s for **4**. As expected,[36] the U_1 values of **3**·2Bu^{t}OH and **4** are smaller than those obtained from fits to eq 3b, and the large $1/\tau_{02}$ values rationalize the importance of excited state pathways to the overall relaxation rate even though U_2 is so large. A comparison of U_1 values becomes the means by which to compare the effective relaxation barriers of different Mn_{12} SMMs in their ground state, and this will be done after the EPR section below.

HFEPR Spectroscopy. To determine the effective giant-spin Hamiltonian parameters for complexes **3** and

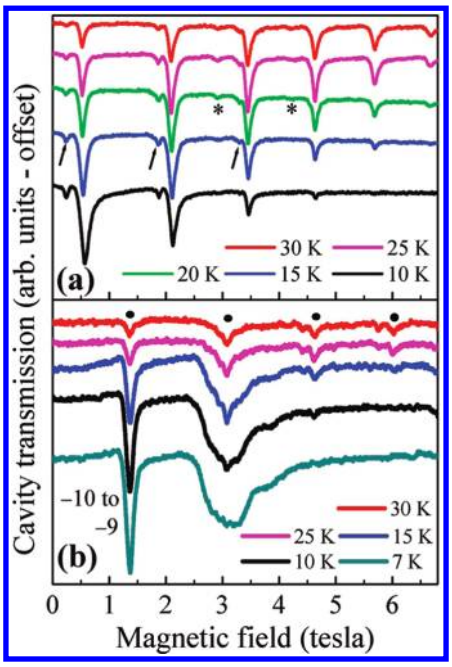

Figure 7. Representative temperature-dependent HFEPR spectra for (a) **3**·2Bu^{t}OH at 294 GHz, with the field aligned close to the magnetic easy-axis; and (b) **4** at 348 GHz, with the field aligned close to the easy-axis of one of the two species in the unit cell. In (a), the arrows identify peaks due to minor species and the asterisks mark transitions involving excited spin states. In (b), the black dots indicate the resonances that are attributed to the aligned molecules and which are used for the simulations in Figure 9.

4, we have carried out extensive multi-HFEPR measurements as a function of magnetic field (frequency), field orientation, and temperature. Figure 7 displays representative temperature dependent HFEPR spectra for (a) complex **3** at 294 GHz, with the field aligned close to the magnetic easy-axis and (b) complex **4** at 348 GHz, with the field aligned close to the easy-axis of one of the two species in the unit cell. Very apparent in Figure 7a are the small satellite peaks (indicated by arrows) on the low-field side of the main series of peaks. The spacing between the main and satellite peaks decreases with increasing field, and the temperature dependence of each satellite peak is similar to the closest strong peak. This type of behavior is indicative of a minor species in the crystals, with a slightly different molecular D value compared to the major species;[37] in contrast to the acetate complex **1**,[38] the minor species have the larger D value in this case, because they possess a larger zero-field intercept (see Figure 8). The ratio of intensities of the peaks attributed to the major and minor species (the smaller peak is ~15% of the spectral weight contained within the two peaks) is in reasonable agreement with the two possibilities due to the $H_2O/Bu^tCH_2CO_2^-$ disorder seen in the crystal structure determination, that is, ~80/20% (see Supporting Information, Figure S2). Additional weak absorptions appear at higher temperatures (marked by asterisks) which likely indicate population of an excited state with a

(37) Lawrence, J.; Yang, E.-C.; Edwards, R.; Olmstead, M. M.; Ramsey, C.; Dalal, N. S.; Gantzel, P. K.; Hill, S.; Hendrickson, D. N. *Inorg. Chem.* **2008**, *47*, 1965.
(38) Waldmann, O.; Carver, G.; Dobe, C.; Sieber, S.; Güdel, H. U.; Mutka, H. *J. Am. Chem. Soc.* **2007**, *129*, 1526.

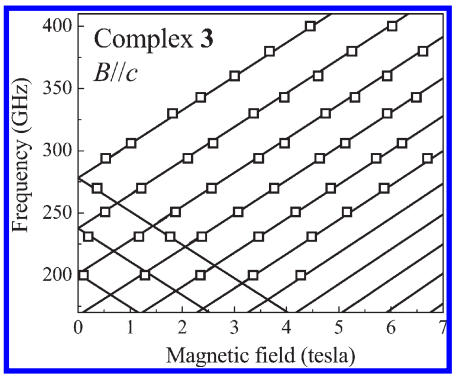

Figure 8. Frequency dependence of HFEPR peak positions (black squares) obtained at 15 K with the field applied approximately parallel to the easy-axes of **3**·2Bu^{t}OH. Superimposed on the data is the best simulation based on eq 5; the obtained ZFS parameters are given in Table 4.

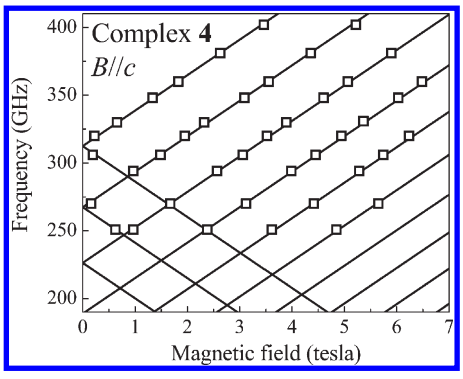

Figure 9. Frequency dependence of HFEPR peak positions (black squares) obtained at 15 K with the field applied approximately parallel to the easy-axes of one of the species of **4**. Superimposed on the data is the best simulation based on eq 5; the obtained ZFS parameters are given in Table 4.

spin value $S < 10$, as has been observed for other Mn_{12} complexes.[39] We discuss the ZFS parameters obtained from these data further below.

The spectra for complex **4** (Figure 7b) are complicated by the presence in the unit cell of two molecular orientations with a 55° easy-axis alignment difference. Thus, it is not possible to align the magnetic field with the easy-axes of both species simultaneously. For this reason, at the lowest temperature in the figure, a sharp symmetric resonance is observed at ~1.35 T, and a much broader peak is observed at 3 T. The former corresponds to the molecules whose easy-axes are approximately aligned with the applied field, while the latter corresponds to the other orientation. On the basis of subsequent fits, we estimate that the misaligned molecules have their easy-axes tilted ~55° away from the applied field, in agreement with the X-ray study. The difference in line width reflects differences in the field dependence of the spectra for the two field orientations, that is, it does not signify any fundamental difference between molecules having different orientations in the unit cell; a more in-depth discussion of EPR spectra of crystals containing differently oriented molecules is available elsewhere.[10n] Peaks assigned to the $S = 10$ state of the aligned molecules of **4** have been highlighted by the black dots in Figure 7b. The higher temperature data were used for subsequent fits so as to minimize complications associated with the misaligned species; although it may not be obvious from Figure 7b which peaks belong to which species, the multifrequency studies greatly simplify this process.

Two-dimensional (2-D) plots of the easy-axis EPR peak positions plotted versus frequency for complexes **3** and **4** are displayed in Figures 8 and 9, respectively. Superimposed upon the data are simulations obtained via solution of the spin Hamiltonian of eq 5.[5f] The solid lines in the two figures were

$$\hat{H} = D\hat{S}_z^2 + B_4^0\hat{O}_4^0 + \mu_B\vec{B}\cdot\vec{\vec{g}}\cdot\hat{S} \qquad (5)$$

generated by computing the energy differences between eigenstates differing by ±1 in spin projection, M_S. The first two terms in eq 5 characterize the second and fourth order axial anisotropies ($\hat{O}_4^0$, which contains $\hat{S}_z^4$, is defined elsewhere[5f]), parametrized by D and B_4^0, respectively. Operators $\hat{S}$ and $\hat{S}_z$ correspond to the total spin and its projection onto the molecular easy- (z-) axis. The final term in eq 5 represents the Zeeman interaction resulting from application of a magnetic field, B, and $\vec{\vec{g}}$ corresponds to the Landé tensor. No transverse ZFS terms have been included in eq 5 because of the complete insensitivity of the high-frequency (> 100 GHz) easy-axis spectra to such interactions (assuming realistic interaction strengths for known Mn_{12} complexes). However, slight misalignment angles ($\theta < 15°$) were included in the simulations because the single-axis rotation measurements do not guarantee perfect easy-axis alignment.

The procedure outlined above provides highly reliable estimates of the axial anisotropy constants for **3** and **4**, and it is these parameters that directly determine U_{EPR}, the theoretical thermodynamic barrier height (U) determined from EPR data.[40] U_{EPR} was calculated as the energy gap between the $M_S = \pm 10$ states and the $M_S = 0$ state, obtained from eq 5 by including both the experimentally obtained second and fourth order axial anisotropy terms, rather than by just calculating the second order $S^2|D|$ value. Values of the ZFS parameters and U_{EPR} obtained for these and other well-known high-symmetry Mn_{12} complexes are listed in Table 4. As stated above, no attempt to measure the transverse (rhombic) ZFS parameters was made in this study; these could be appreciable because of the low symmetry of these complexes, especially **3**. However, their evaluation represents a significant undertaking on the basis of single-crystal measurements, and is beyond the scope of the present investigation.

Remarkably, the uniaxial anisotropy D (and also U_{EPR}) determined from EPR for complex **4** turns out to be greater than for any previously studied Mn_{12} SMM. The next closest is $[Mn_{12}O_{12}(O_2CCH_2Br)_{16}(H_2O)_4]\cdot 4CH_2Cl_2$ (Mn_{12}−BrAc);[26,36] U_{EPR} for **4** is ~4.5% larger, as is D. Table 4 also compares the effective kinetic barrier U_{eff} (U_1) of **3**·2Bu^{t}OH and **4**, determined from a double-exponential fit of the AC susceptibility data (see above),[36] with those obtained for high-symmetry Mn_{12} complexes

(39) Petukhov, K.; Hill, S.; Chakov, N. E.; Christou, G. *Phys. Rev. B* **2004**, *70*, 054426.

(40) Redler, G.; Lampropoulos, C.; Datta, S.; Koo, C.; Stamatatos, T. C.; Chakov, N. E.; Christou, G.; Hill, S. *Phys. Rev. B* **2009**, *80*, 094408.

Table 4. Comparison of ZFS Parameters, U_{EPR} and U_{eff} for Several Recent Mn_{12} Complexes

complex	ZFS (K)[a]	D (K)	B_4^0 ($\times 10^{-5}$ K)	U_{EPR} (K)	U_{eff} (K)[b]
$[Mn_{12}O_{12}(O_2CMe)_{16}(H_2O)_4]$ (**1**)[c]	14.12(5)	−0.655(9)	−2.9(5)	66.2(13)	62(0.5)
$[Mn_{12}O_{12}(O_2CCH_2Br)_{16}(H_2O)_4]\cdot 4CH_2Cl_2$	14.90(5)	−0.674(5)	−3.6(3)	68.2(7)	66(1)
$[Mn_{12}O_{12}(O_2CCH_2Bu^t)_{16}(MeOH)_4]$ (**2**)[c]	14.73(5)	−0.665(9)	−3.6(5)	67.3(13)	63(1)
$[Mn_{12}O_{12}(O_2CCH_2Bu^t)_{16}(Bu^tOH)(H_2O)_3]$ (**3**)[c]	13.35(5)	−0.626(3)[d]	−2.50(15)	63.2(7)	54.8(1.7)[e]
$[Mn_{12}O_{12}(O_2CCH_2Bu^t)_{16}(C_5H_{11}OH)_4]$ (**4**)	14.99(5)	−0.705(3)	−2.74(15)	71.2(7)	67.9(9)[e]

[a] Experimental energy gap between the $M_S = \pm 10$ and ± 9 levels determined directly from the HFEPR data. [b] U_1 from a double-exponential fit to eq 4; see the text and ref 36 for explanation. [c] Full formulas: **1**·2$MeCO_2H$·4H_2O, **2**·MeOH, **3**·2Bu^tOH. [d] Value of D for the minor species is ∼2% higher. [e] Values obtained using a single-exponential Arrhenius fit (eq 3b) are 62.6 and 71.2 K for **3**·2Bu^tOH and **4**, respectively, as given in the text.

studied recently: the value for **4** is larger than that for the Mn_{12}−BrAc complex and the others: $U_{eff} = 67.9(9)$ K for **4** versus 66(1) K for Mn_{12}−BrAc, the next largest. Indeed, on the basis of the EPR studies and the careful analysis of the AC susceptibility data, we conclude that **4** possesses the largest barrier U_{eff} (U_1) yet obtained for a Mn_{12} SMM.

In spite of its rhombic space group ($P2_1/c$) and virtual point group (D_2) symmetry, the $Mn_{12}O_{12}$ core of **4** is virtually indistinguishable from the high symmetry (tetragonal space group and imposed S_4 point group) Mn_{12} complexes.[14] In particular, the JT axes are oriented in a pseudo-S_4 fashion; they are also rather parallel, thus likely resulting in a near maximal projection of the Mn^{III} single-ion anisotropy onto the molecular spin $S = 10$ state, and to negligible rhombic ZFS ($E \sim 0$). In addition, several factors hint at the possibility that the ground $S = 10$ state in **4** may be more isolated from excited states in comparison to previously studied high-symmetry Mn_{12} complexes (see below). The interaction between spin-multiplets (S-mixing) is known to compress the magnetization barrier, with the magnitude of B_4^0 providing a rough measure of the compression.[41−43] Consequently, the better isolation of the $S = 10$ state in **4** may account for its record D and effective barrier, U_{eff}, for a Mn_{12} SMM.

In contrast to **4**, the magnetic core of complex **3** is more distorted (Figure 3), as discussed above, with very little resulting symmetry. In addition, four of the JT axes are significantly tilted toward the plane of the molecule. It is thus no surprise that the measured axial anisotropy is significantly smaller for this complex, giving $U_{EPR} = 63.2(7)$ K and $U_{eff} = U_1 = 54.8(17)$ K, as determined by the double-exponential method.[36] The reduction in U_{EPR} is most likely due to the significant tilting of four Jahn−Teller axes away from the molecular z (easy-axis) direction, decreasing $|D|$. The further reduction in U_{eff} can be attributed to the low symmetry of the core, which is expected to lead to significant rhombic anisotropy (not measured) and fast tunneling between states well below the top of the barrier,[44] that is, to a reduction in the kinetic barrier (U_{eff}).

We conclude by commenting further on the isolation of the $S = 10$ state in complex **4**. Several subtle features of the measurements reported here have led us to this

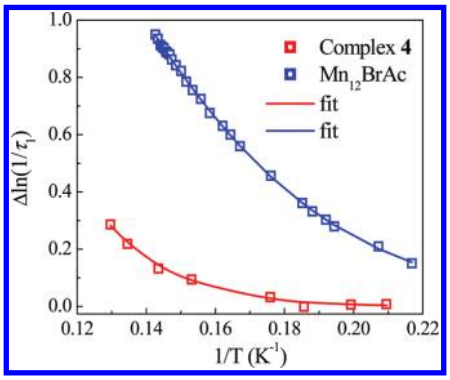

Figure 10. Comparison of the non-linear deviation from Arrhenius behavior for complex **4** and Mn_{12}BrAc. The solid curves are double-exponential fits to the data based on a procedure described in ref 36.

conclusion. The first is the fact that the fourth order anisotropy is much smaller for **4** compared with other high-symmetry Mn_{12} complexes: $B_4^0 = -2.74 \times 10^{-5}$ K in **4**, and is 30% larger in the high symmetry Mn_{12}−BrAc and Mn_{12}−Bu^tAc complexes.[40] Recent work has shown that this parameter provides a measure of the degree of state mixing between spin multiplets which, in turn, may crudely be taken as a gauge of the proximity of excited spin multiplets to the ground state.[41−43] In addition, as described above and in ref 36, the non-linearity of Arrhenius plots such as those in Figure 6 is due to relaxation via excited state pathways; the degree of curvature and the resulting magnitude of U_2 thus constitute a measure of the proximity of excited states.[36] It is thus pertinent to note the very large $U_2 = 123(18)$ K for **4**, which is consistent with a better isolated ground state and a resulting near-linear Arrhenius plot—the latter also rationalizes the large fit uncertainty in U_2. In Figure 10, we compare the non-linear contributions to the Arrhenius plots for complex **4** and Mn_{12}−BrAc (i.e., the U_2 terms of eq 4).[36] In both cases, the linear contribution corresponding to the $T \rightarrow 0$ K extrapolation of U_{eff} (U_1) has been subtracted ($U_{eff} = 67.9(9)$ K for **4**, and 66(1) K for Mn_{12}−BrAc), so that the deviation from the $\Delta\ln(1/\tau_1) = 0$ line in Figure 10 is a measure of the non-linear behavior (the U_2 term). Alternatively, this deviation $\Delta\ln(1/\tau_1)$ may be viewed as a measure of the contribution of excited states to the relaxation. As can clearly be seen, the deviation for complex **4** is far smaller than for Mn_{12}−BrAc, and the temperature at which the deviation becomes noticeable is considerably higher for **4**. This, together with the correlation with the B_4^0 parameter, lends support to the conclusions in reference 36 and strongly suggests that the $S = 10$ state in **4** is better isolated from excited spin states in comparison to other well-studied Mn_{12} complexes.

(41) Wilson, A.; Lawrence, J.; Yang, E.-C.; Nakano, M.; Hendrickson, D. N.; Hill, S. *Phys. Rev. B* **2006**, *74*, R140403.
(42) Datta, S.; Waldmann, O.; Kent, A. D.; Milway, V. A.; Thompson, L. K.; Hill, S. *Phys. Rev. B* **2007**, *76*, 052407.
(43) Feng, P. L.; Koo, C.; Henderson, J.; Manning, P.; Nakano, M.; del Barco, E.; Hill, S.; Hendrickson, D. N. *Inorg. Chem.* **2009**, *48*, 3480.
(44) Hill, S.; Murugesu, M.; Christou, G. *Phys. Rev. B* **2009**, *80*, 174416.

The above statement also provides a possible explanation for the larger uniaxial anisotropy found in **4**. At the present time, it is not easy to rationalize this finding on the basis of the known structures, and small differences in JT axis elongations and orientations between them and **4**. Another possible explanation may be the 2:2 distribution of the alcohol molecules on two Mn^{III} ions (Mn9, Mn11) whereas in most other Mn_{12} complexes studied in detail by HFEPR the terminal ligands are distributed in a 1:1:1:1 fashion on four alternating Mn^{III} ions. The concentration of two neutral ligands on two of the Mn^{III} ions, and thus two charged carboxylates at the other two corresponding Mn^{III} atoms, should lead to changes in the single-ion anisotropies, which might, in turn, change their projection onto the molecular anisotropy sufficiently to yield the observed result. It will take detailed HFEPR studies on additional examples of Mn_{12} complexes with a 2:2 distribution of neutral solvent molecules to probe this point further.

Conclusions

The synthesis of two new Mn_{12} derivatives bearing bulky $Bu^tCH_2CO_2^-$ ligands and terminally coordinated alcohol groups has been achieved using a one-step procedure starting from readily accessible complex **1**. This procedure could no doubt be employed with a variety of alcohol groups, but in the present work we have used Bu^tOH and *n*-pentanol, which are both large but with significantly different steric bulk, and investigated their influence on the structure and properties of the resulting Mn_{12} complexes. Indeed, this work has demonstrated that the use of bulky Bu^tOH, and by implication other bulky alcohols, may provide a convenient means of imposing ligand-induced distortions onto the $[Mn_{12}O_{12}]$ core, since even the single Bu^tOH bound in $\mathbf{3}\cdot 2Bu^tOH$ can only be accommodated with significant distortion of the molecule and its magnetic core, whereas $[Mn_{12}O_{12}(O_2CCH_2Bu^t)_{16}(MeOH)_4]$ has imposed S_4 symmetry. In contrast to $\mathbf{3}\cdot 2Bu^tOH$, four *n*-pentanol groups are bound in **4**, which has virtual D_2 symmetry.

Both $\mathbf{3}\cdot 2Bu^tOH$ and **4** are SMMs, as indicated by AC susceptibility studies, and single-crystal HFEPR spectra have provided important information about their magnetization barriers. They have shown that the thermodynamic barrier (U_{EPR}), determined from the second and fourth order axial anisotropy parameters measured by EPR, is 63.2 K for $\mathbf{3}\cdot 2Bu^tOH$ and 71.2 K for **4**. Thus, the ligand-induced distortions in $\mathbf{3}\cdot 2Bu^tOH$ serve to decrease U_{EPR}, whereas **4** has been found to be the Mn_{12} complex with the highest thermodynamic barrier U_{EPR} yet, a few degrees kelvin less than the U_{EPR} for a Mn_6 compound.[45] It also has the highest kinetic barrier U_{eff} to date for a Mn_{12} SMM, measured as U_1 by the recently published double-exponential Arrhenius fit;[36] although the number of Mn_{12} complexes that have been analyzed by the latter method is still limited (Table 4), they do include the crytallographically axial (tetragonal space group) examples that in general display the largest barriers. We believe this is due to a combination of factors, including the 2:2 distribution of alcohol groups in **4**, and a more isolated $S = 10$ ground state that minimizes spin-mixing with excited states.

The results of this work establish the modification of bound alcohol groups as a new approach for engineering changes to the Mn_{12} family of SMMs, including increasing the magnetization relaxation barriers. In addition, the use of bulky carboxylates such as $Bu^tCH_2CO_2^-$ ensures good isolation of adjacent magnetic cores in such studies, and is encouraged as beneficial. Further studies are in progress.

Acknowledgment. This work was supported by the National Science Foundation (Grants CHE-0414555, CHE-0910472, DMR-0239481, and DMR-0804408).

Supporting Information Available: X-ray crystallographic files in CIF format for complexes **3** and **4**, and additional information as noted in the text. This material is available free of charge via the Internet at http://pubs.acs.org.

(45) Inglis, R.; Jones, L. F.; Milios, C. J.; Datta, S.; Collins, A.; Parsons, S.; Wernsdorfer, W.; Hill, S.; Perlepes, S. P.; Piligkos, S.; Brechin, E. K. *Dalton Trans.* **2009**, 3403.